Subnanometer Motion of Cargoes Driven by Thermal Gradients along Carbon Nanotubes
Author(s): Amelia Barreiro, Riccardo Rurali, Eduardo R. Hernández, Joel Moser, Thomas Pichler, László Forró and Adrian Bachtold
Source: *Science*, New Series, Vol. 320, No. 5877 (May 9, 2008), pp. 775-778
Published by: American Association for the Advancement of Science
Stable URL: http://www.jstor.org/stable/20054685
Accessed: 28-09-2016 17:15 UTC

We have demonstrated a method to realize conditional dynamics in a system of two CQDs. The interaction mechanism relies on the tunnel coupling, which can lead to conditional energy shifts that are much larger than those provided by dipole-dipole interactions. More importantly, this tunnel-coupling–mediated interaction can be effectively tuned by changing the energy level detuning via the gate voltage, and it can be optically gated in sub-picosecond time scales by creation of an exciton.

References and Notes

1. P. M. Petroff, A. Lorke, A. Imamoglu, *Phys. Today* **54**, 46 (2001).
2. X. Li *et al.*, *Science* **301**, 809 (2003).
3. M. O. Scully, M. S. Zubairy, *Quantum Optics* (Cambridge Univ. Press, Cambridge, 1997).
4. R. Hanson, L. P. Kouwenhoven, J. R. Petta, S. Tarucha, L. M. K. Vandersypen, *Rev. Mod. Phys.* **79**, 1217 (2007).
5. M. Atatüre *et al.*, *Science* **312**, 551 (2006); published online 5 April 2006 (10.1126/science.1126074).
6. J. Berezovsky *et al.*, *Science* **314**, 1916 (2006); published online 9 November 2006 (10.1126/science.1133862).
7. M. Atatüre, J. Dreiser, A. Badolato, A. Imamoglu, *Nat. Phys.* **3**, 101 (2007).
8. M. Kroner *et al.*, preprint available at http://arxiv.org/abs/0710.4901.
9. M. H. Mikkelsen, J. Berezovsky, N. G. Stoltz, L. A. Coldren, D. D. Awschalom, *Nat. Phys.* **3**, 770 (2007).
10. D. Loss, D. P. DiVincenzo, *Phys. Rev. A* **57**, 120 (1998).
11. J. R. Petta *et al.*, *Science* **309**, 2180 (2005); published online 1 September 2005 (10.1126/science.1116955).
12. H. J. Krenner *et al.*, *Phys. Rev. Lett.* **94**, 057402 (2005).
13. E. A. Stinaff *et al.*, *Science* **311**, 636 (2006); published online 11 January 2006 (10.1126/science.1121189).
14. S. Fält *et al.*, *Phys. Rev. Lett.* **100**, 106401 (2008).
15. T. Calarco, A. Datta, P. Fedichev, E. Pazy, P. Zoller, *Phys. Rev. A* **68**, 012310 (2003).
16. C. Hettich *et al.*, *Science* **298**, 385 (2002); published online 5 September 2002 (10.1126/science.1075606).
17. T. Unold, K. Mueller, C. Lienau, T. Elsaesser, A. D. Wieck, *Phys. Rev. Lett.* **94**, 137404 (2005).
18. M. Bayer *et al.*, *Phys. Rev. B* **65**, 195315 (2002).
19. D. Gammon, E. S. Snow, B. V. Shanabrook, D. S. Katzer, D. Park, *Phys. Rev. Lett.* **76**, 3005 (1996).
20. In principle, states $|1\rangle$ or $|5\rangle$ or $|6\rangle$ and $|7\rangle$ could be split because of electron tunneling, but each of these resonances will only occur at substantially different gate voltages because of the fact that the tunneling strength is much smaller than the relevant Coulomb interaction energies.
21. R. J. Warburton *et al.*, *Nature* **405**, 926 (2000).
22. In the inset, the mixing of the bright X_y^0 with the indirect exciton is hardly resolved. Clearly visible is the anticrossing of the indirect exciton with the dark X_y^0, which becomes bright because of the mixing (*14*).
23. B. Alén, F. Bickel, K. Karrai, R. J. Warburton, P. M. Petroff, *Appl. Phys. Lett.* **83**, 2235 (2003).
24. The gate voltage scale for the absorption measurements is slightly different from that of PL because of technical reasons (*28*).
25. To illustrate the observed effect clearly, the intensity of the probe laser is chosen such that it saturates the corresponding ground state transition, whereas the pump laser is set to five times the saturation intensity.
26. In addition to the strong shifted red absorption that occurs for a resonant blue laser (around 1334.63 meV), we also see a weak red absorption around 1261.04 meV even when the blue laser is not resonant. This effect, which is not present when the blue laser is turned off, indicates that even a nonresonant blue laser has a small probability to lift the tunneling resonance between states $|2\rangle$, $|3\rangle$, and $|4\rangle$. This is most likely due to the creation of charges in nearby impurity sites, which can shift the effective gate voltage felt by the CQD. Also, a faint diagonal absorption line is visible around the shifted resonance, which is due to two-photon resonance between states $|1\rangle$ and $|6\rangle$.
27. We have assumed that all excited states are lifetime-broadened.
28. Materials and methods are available on *Science* Online.

29. This work is supported by National Centre of Competence in Research Quantum Photonics (NCCR QP), research instrument of the Swiss National Science Foundation (SNSF), and European Union Research Training Network Engineering, Manipulation, and Characterization of Quantum States of Matter and Light (EMALI). The authors thank K. Weiss for experimental assistance.

Supporting Online Material

www.sciencemag.org/cgi/content/full/320/5877/772/DC1
Materials and Methods
Figs. S1 to S4
References

18 January 2008; accepted 1 April 2008
10.1126/science.1155374

Subnanometer Motion of Cargoes Driven by Thermal Gradients Along Carbon Nanotubes

Amelia Barreiro,[1] Riccardo Rurali,[2] Eduardo R. Hernández,[3]* Joel Moser,[1] Thomas Pichler,[4] László Forró,[5] Adrian Bachtold[1]*

An important issue in nanoelectromechanical systems is developing small electrically driven motors. We report on an artificial nanofabricated motor in which one short carbon nanotube moves relative to another coaxial nanotube. A cargo is attached to an ablated outer wall of a multiwalled carbon nanotube that can rotate and/or translate along the inner nanotube. The motion is actuated by imposing a thermal gradient along the nanotube, which allows for subnanometer displacements, as opposed to an electromigration or random walk effect.

There is a growing effort in the scientific community to design and fabricate ever more versatile nanoelectromechanical systems (NEMS) (*1*). Because carbon nanotubes are very small, mechanically robust, and chemically inert, they have attracted considerable interest as NEMS components. In addition, their one-dimensional tubular shape offers a natural track for motion. This tubular shape restricts the motion (typically translation or rotation) to only a few degrees of freedom, much as bearings do in everyday machines. The tubular track has been the key component for the fabrication of nanotube-based switches (*2*), rotors (*3*, *4*), and mass conveyors (*5*–*7*).

A second generation of nanotube-based motors has been envisaged that takes advantage of the atomic corrugation for a new class of tracks (*8*, *9*). Because the atoms in a nanotube can be arranged in many different configurations, as defined by its chirality, such motors are expected to be quite versatile. For example, a gold nanoparticle confined inside a nanotube is expected to move along a helical orbit around the nanotube axis; this orbit can take different angles and periodicities, which are controlled by the nanotube chirality (*10*, *11*).

The motion of two coaxial nanotubes relative to one another offers additional possibilities, because it combines a pair of chiralities. The track is given by the mutual atomic interaction between the nanotubes. In some cases, the track follows energy minima that can consist of helical orbits ranging from pure rotation to pure translation. In other cases, it contains local minima and maxima, which can be arranged, for example, as a twisted chessboard-like pattern (see some examples in Fig. 1, D to F) (*8*). This flexibility of the energy surface for motion is expected to provide the framework to explore various motion-related phenomena at the nanoscale, such as the ratchet effect (*12*, *13*), vanishingly small friction (*14*), friction resonances (*15*, *16*), and thermal gradient–induced motion (*10*, *11*). However, nanotube motors controlled by the atomic corrugation remain to be experimentally demonstrated.

We report two advances on a nanotube-based motor designed so that motion occurs between two coaxial nanotubes. First, the atomic interaction between the nanotubes is shown to generate distinct kinds of motion for different devices: namely, rotation and/or translation along the nanotube axis. Second, we show that the motion is driven by a thermal gradient. More specifically, the thermal gradient generates a phononic current in one nanotube that hits and drags the second tube. Both findings hold promise for practical use in future NEMS.

[1]Centre d'Investigacions en Nanociencia i Nanotecnologia (Consejo Superior de Investigaciones Científicas–Institut Català de Nanotecnologia) and Centro Nacional de Microelectrónica, Campus de la Universitat Autònoma de Barcelona (UAB), E-08193 Bellaterra, Spain. [2]Departament d'Enginyeria Electrònica, UAB, E-08193 Bellaterra, Spain. [3]Institut de Ciència de Materials de Barcelona, Campus UAB, E-08193 Bellaterra, Spain. [4]Faculty of Physics, University of Vienna, Strudlhofgasse 4, 01090 Wien, Austria. [5]Ecole Polytechnique Fédérale de Lausanne, CH-1015 Lausanne, Switzerland.

*To whom correspondence should be addressed. E-mail: adrian.bachtold@cnm.es (A.B.); ehe@icmab.es (E.R.H.)

Devices were constructed by means of standard nanofabrication techniques. Multiwalled carbon nanotubes (MWNTs), synthesized by arc-discharge evaporation, were deposited onto an oxidized silicon substrate. Electron-beam lithography and Cr/Au evaporation were used to attach electrodes to an individual nanotube and to pattern a plate in the middle of the nanotube that plays the role of the cargo. A few outer walls of the MWNT were selectively removed via the electrical-breakdown technique, which consists of passing a large current through the MWNT (*17*–*19*). The device is completed by suspending the nanotube and the cargo by means of a wet etching step.

This fabrication process created a motor that consists of a mobile element, which can move along and/or rotate around the axis of the suspended nanotube. The mobile metal cargo is attached to at least one short shell that can slide with respect to the other shells (Fig. 1C). The electrical-breakdown technique does not remove the shell(s) below the metal cargo, probably because the metal plate efficiently absorbs the heat generated in this portion of the tube, which prevents or at least delays the tube oxidation in this part. This mode of attachment can be inferred, because it is possible to move the metal cargo several times back and forth by means of an atomic force microscope (AFM) (Fig. 1, A and B). In contrast, the devices not engineered with the electrical-breakdown technique do not allow for such a manipulation (*20*). The cargo stays immobile until it is suddenly detached from the nanotube when the force applied by the tip becomes too large. Further discussion is provided in (*21*) and elsewhere in the supporting online material (SOM).

The motion of the cargo can also be driven by passing an electron current through the nanotube (without intervention of an AFM). The current has to be large (~0.1 mA) to make this happen. High currents likely cause sufficient dissipation to clean the surface from contaminants and help prevent dangling bonds from obstructing the motion. Previous experiments have shown that the presence of such contaminants alters the motion in a stochastic way (*4*, *22*, *23*). In our case, once the mobile element is free to move, the motion is often observed to be markedly regular and to be oriented toward a specific direction. For some devices, the cargo rotates around the nanotube (Fig. 2); for others, it moves along the nanotube axis (Fig. 3). The SOM contains a selection of videos (movies S2 to S4) and a summary table (table S1) on the motion observed for 11 different devices.

These results can be understood by considering the energy barrier for the relative motion between two coaxial nanotubes. As discussed above, the interaction between atoms of the two tubes generates an energy surface that restricts the motion along specific tracks, which can be translational and rotational (Fig. 1, D to F). In the general case, the easy direction will have both components. However, the motion appears most often to be purely rotational even if it is not, because a small rotation component generates a large deflection of the cargo, whereas a small translation component does not.

Occasionally, the cargo moves in a stepwise fashion, such as the rotational motion shown in Fig. 2. The angle of rotation is markedly constant for the different steps [about 7° (Fig. 2B)], which corresponds to a displacement $a_0 \approx 0.4$ nm along the track of the nanotube, given that its diameter is 7 nm. Such stepwise motion suggests that the cargo must overcome a series of periodic barriers (Fig. 2C). The observed motion is always toward the same direction, which differs from the motion of the ratchet effect (*13*, *24*) that is often used to describe molecular motors. There, the direction of motion fluctuates in time (a net directed displacement is obtained on average).

The energy of the periodic barriers can be estimated by noting that the temperature of the nanotube is very high. The high current flowing through the nanotube results in a high dissipation, which increases the temperature (*25*). The gold cargo, which initially has a rectangular shape, is often observed to melt and to transform into a ball, as shown in Fig. 3 (see also fig. S3). This result suggests that the temperature T approaches the melting temperature of gold (about 1300 K). We can obtain a rough estimate of the barrier height ΔE as

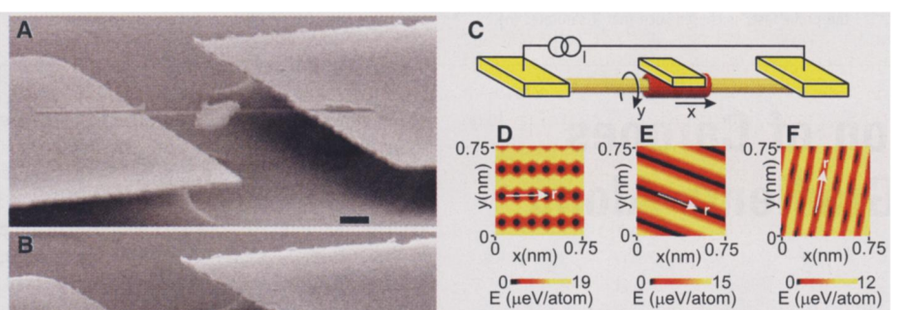

Fig. 1. Experimental setup. (**A** and **B**) Scanning electron microscope (SEM) images of one device where the central object attached to nanotube in (A) has been moved via an AFM tip. Scale bar in (A), 300 nm. (**C**) Schematic of the nanotube motor and its degrees of freedom. The outer (red) nanotube moves with respect to the inner (yellow) nanotube. *I*, the current. (**D** to **F**) Shape of the energy barrier for the relative motion between two coaxial nanotubes: (5,5)/(10,10), (29,9)/(38,8), and (27,12)/(32,17), respectively. The diameters of the inner tubes are 0.67, 2.7, and 2.7 nm, respectively. The white arrows indicate the easy axis of motion (*r*). The motion is modulated by a series of small periodic barriers in (D) and (F), whereas vanishingly small friction is expected in (E).

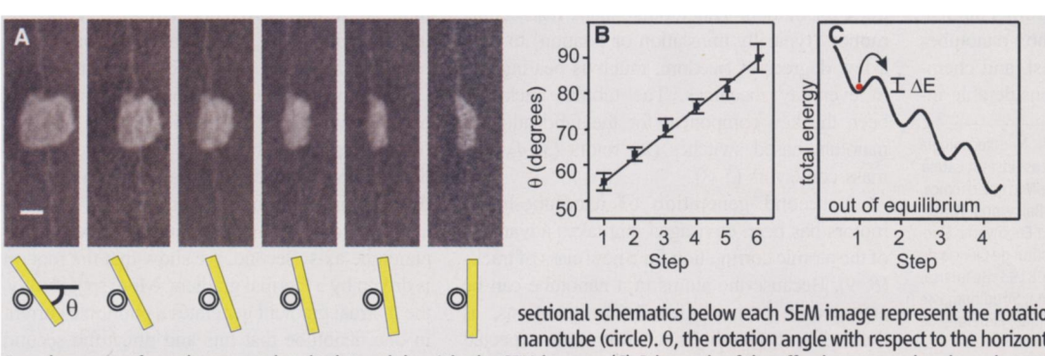

Fig. 2. Rotational motion. (**A**) Top-down SEM images where the gold cargo lying on the movable nanotube is rotating stepwise. The average time for a stepwise rotation to occur is 2.3 s (movie S3). The motion is driven by a 0.07-mA current through the nanotube, and the voltage is 2.3 V. Images are obtained with 10-keV electrons at a pressure of 10^{-6} mbar. Scale bar, 100 nm. The cross-sectional schematics below each SEM image represent the rotation of the plate (rectangle) around the nanotube (circle). θ, the rotation angle with respect to the horizontal. (**B**) Angle of rotation for each step. Error bars come from the uncertainty in determining θ in the SEM images. (**C**) Schematic of the effective energy barriers along the easy axis of motion. The red ball describes the movable nanotube.

follows. If we assume that the motion is in the hindered regime under the conditions present in our experiments, and if we neglect entropic contributions caused by the atomic motion (*26*), we have

$$\Gamma = \frac{\omega}{2\pi} e^{-\Delta E/kT} \quad (1)$$

with motion rate Γ and attempt frequency ω, where k is Boltzmann's constant. The precise values of Γ and ω are not important, because they appear as logarithmic terms in ΔE. Taking $\Gamma \approx 1$ Hz, using the approximation $\omega = \sqrt{\frac{\Delta E/a_0^2}{m}}$ with the mass m of the cargo, and using the result that the barrier height is proportional to the contact area (*8*), we obtain a barrier height of ~17 μeV per atom.

We now analyze the observed stepwise motion described above in light of the interaction between two coaxial nanotubes. As discussed previously, the direction of motion follows a main valley of minimum energy. Along this valley, the energy can be either roughly constant or periodically modulated by a series of barriers (Fig. 1, D to F) (*8*). In the former case, the friction is expected to be vanishingly small when neglecting the vibrational motion of the atoms, whereas in the latter case, the motion can be stepwise. For example, as for the (27,12) and the (32,17) nanotubes shown in Fig. 1F, a series of local minima appears along the valley at regular intervals of 0.26 nm, separated by a barrier height of 3 μeV per atom. The stepwise motion observed in Fig. 2 is attributed to such a periodic modulation of the energy along the easy direction of motion. Note that the actual values of the separation and the barrier height are chirality- and diameter-dependent. In addition, the effective barrier that we obtain from our experiments contains an entropic contribution from the vibrational motion of the atoms, which is not considered in this simple model.

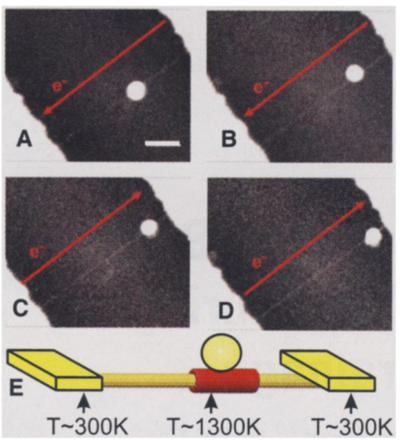

Fig. 3. Translational motion. (**A** to **D**) Top-down SEM images where the gold cargo (sphere) is moving along the nanotube. The direction of motion remains the same as the polarity of the current (red arrow) is reversed, which rules out an electromigration effect as the actuation mechanism. In (A) and (B), the current is 0.11 mA (3.1 V), whereas in (C) and (D), it is −0.13 mA (−3.6 V). Scale bar in (A), 400 nm. (**E**) Schematic illustration of the temperature along the nanotube caused by Joule heating. The motion of the cargo is driven from the hot spot to the cold region and is unaffected by the inversion of the current polarity.

Let us now discuss the underlying mechanism of the actuation. At first glance, it may be natural to attribute the driving force to the electrical current, as in electromigration, where electrons move atomic impurities through collisions and momentum transfer. However, upon reversing the direction of the current, the cargo continues to displace in the same direction as before (Fig. 3 and movie S4). This finding rules out an electromigration effect as the source of the observed dynamics. We emphasize that the rotational motion is neither the result of the magnetic field induced by the current passing through the nanotube—because the rotation can be right-handed or left-handed, depending on the device (*21*)—nor the result of a stray electric field effect, because the metal plate stays immobile for high-resistive devices even if a high voltage is applied (*21*).

We attribute the driving mechanism to the large thermal gradient along the nanotube. As previously discussed, the gold cargo is often observed to melt, which is indicative of a very high temperature. Nevertheless, the nanotube does not heat up homogeneously, because the heat is evacuated through the electrodes (Fig. 3E). The hottest spot of the device is at (or near) the midpoint of the suspended nanotube, whereas the temperature at the interface with the electrodes is expected to be near room temperature, as was recently measured by Begtrup *et al.* (*27*, *28*). Assuming that the temperature varies between 1300 and 300 K along the nanotube, the thermal gradient is as high as 1 K/nm, given the typical dimensions of our devices.

In the presence of a thermal gradient along the nanotube, there will be a net current of phononic excitations traveling from the hot spot toward the cooler regions: that is, from the midpoint of the suspended nanotube toward the electrodes. These phononic excitations will interact with and transfer momentum to the mobile element, and as a consequence, the cargo will move toward the closest electrode (*29*). Notice that the shape of the thermal gradient is independent of the direction of the electron current, which explains why the cargo does not change direction upon reversing the electron polarity.

This process can be regarded as the reverse of the heat dissipation that occurs in friction: When two objects slide in contact, some of the kinetic energy is dissipated as phononic excitations caused by the interface corrugation. In our experimental setting, in contrast, we induce a net current of phononic excitations that collides with the mobile element. In this scattering process, some of the vibrational energy is transformed into kinetic energy of the mobile element.

In order to substantiate our claim that the thermal gradient is indeed the driving mechanism, we have performed molecular dynamics simulations (Fig. 4A). We take the inner nanotube to be long and subject to a temperature gradient (typically a few kelvin degrees per nanometer), whereas the outer nanotube is short (typically 5 nm) and plays the role of the mobile element. Following the methodology of Saito *et al.* (*8*), we model the inter-nanotube atomic interactions by means of a simple Lennard-Jones pair potential and the intra-nanotube interactions by means of the Tersoff potential for carbon (*30*). Care is taken so that, initially, the outer nanotube has no net center-of-mass velocity, in order to avoid any bias in its dynamics. Full details of our simulations are provided in (*21*). In all our calculations, considering different combinations of inner-outer nanotubes and different diameters, we invariably find a net displacement toward the cold region. In addition, the simulations show that, depending on the nanotube pair, the motion can be translation, rotation, or a mixture of both (Fig. 4, B and C).

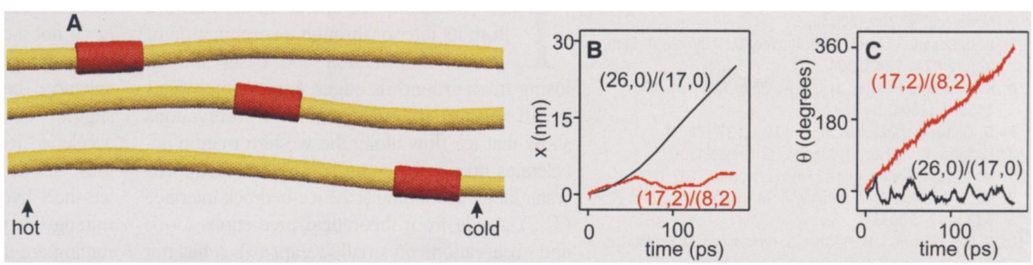

Fig. 4. Molecular dynamics simulations describing the thermal gradient actuation. (**A**) Snapshots of the device that show the motion of the outer (red) nanotube toward the cold end. The temperature gradient along the inner (yellow) nanotube is 7 K/nm, which is imposed by keeping the cold end at 300 K and the hot end at 1000 K. The snapshots are separated by 80 ps, the chiralities are (26,0)/(17,0), and the outer nanotube is 5 nm long. (**B** and **C**) Translational and rotational components of the motion as a function of time for two pairs of chiralities: (17,2)/(8,2) in red and (26,0)/(17,0) in black. The temperature gradient is 1 K/nm.

The motion in these simulations can be markedly fast, up to about 10^8 μm/s. By comparison, the velocity of kinesin-propelled microtubules is typically about 1 μm/s, whereas actin mobility can reach speeds up to 10 μm/s (*31*). However, the velocity that we observe experimentally is only up to about 1 μm/s (*21*). The large difference in velocity between the experiments and simulations is attributed to the difference in the system dimensions. Considering that the number of atoms of the outer nanotube used in the experiments is about 100 times as large as the number of atoms of the nanotube used in the simulations, and taking Eq. 1 with typical values for the temperature and the barrier height (for example, 1300 K and 17 μeV per atom), we obtain a factor of about eight orders of magnitude difference for the velocity, which is consistent with the mismatch between the experiments and simulations. Because our calculation capabilities do not allow speeds down to 1 μm/s to be reached, a direct comparison of the experiments and simulations cannot be made.

Although the temperature in our experiments may appear to be high, it should be possible to reduce it, which would be convenient for certain applications. To achieve this goal, researchers must make the dimensions of the movable nanotube narrower and shorter in order to reduce the barrier height. Another possible solution would be to selectively excite specific phonon modes, so that the average temperature of the phonon bath is lower. Indeed, not all of the phonon modes are expected to interact in the same way with the movable nanotube, and some are likely to be more effective in transferring momentum, such as the breathing modes.

The actuation by means of thermal gradients has obvious potential for NEMS applications. Thermal gradients could be used to drive the flow of fluids inside nanotubes or in nanofluidic devices or used for drug delivery by nanosyringes. The thermal gradient actuation may also be applied to bioengineered nanopores via, for example, the heat generated from the hydrolysis of adenosine triphosphate molecules. Using methods to align nanotubes on substrates, researchers should be able to fabricate arrays of orientationally ordered nanotube-based thermal motors.

References and Notes

1. M. L. Roukes, *Phys. World* **14**, 25 (2001).
2. V. V. Deshpande *et al.*, *Nano Lett.* **6**, 1092 (2006).
3. A. M. Fennimore *et al.*, *Nature* **424**, 408 (2003).
4. B. Bourlon, D. C. Glattli, C. Miko, L. Forro, A. Bachtold, *Nano Lett.* **4**, 709 (2004).
5. B. C. Regan, S. Aloni, R. O. Ritchie, U. Dahmen, A. Zettl, *Nature* **428**, 924 (2004).
6. K. Svensson, H. Olin, E. Olsson, *Phys. Rev. Lett.* **93**, 145901 (2004).
7. D. Golberg *et al.*, *Adv. Mater.* **19**, 1937 (2007).
8. R. Saito, R. Matsuo, T. Kimura, G. Dresselhaus, M. S. Dresselhaus, *Chem. Phys. Lett.* **348**, 187 (2001).
9. Yu. E. Lozovik, A. V. Belikov, A. M. Popov, *Phys. Lett. A* **313**, 112 (2003).
10. P. A. E. Schoen, J. H. Walther, S. Arcidiacono, D. Poulikakos, P. Koumoutsakos, *Nano Lett.* **6**, 1910 (2006).
11. P. A. E. Schoen, J. H. Walther, D. Poulikakos, P. Koumoutsakos, *Appl. Phys. Lett.* **90**, 253116 (2007).
12. Z. C. Tu, X. Hu, *Phys. Rev. B* **72**, 033404 (2005).
13. R. D. Astumian, P. Hanggi, *Phys. Today* **55**, 33 (2002).
14. A. N. Kolmogorov, V. H. Crespi, *Phys. Rev. Lett.* **85**, 4727 (2000).
15. P. Tangney, M. L. Cohen, S. G. Louie, *Phys. Rev. Lett.* **97**, 195901 (2006).
16. J. Servantie, P. Gaspard, *Phys. Rev. B* **73**, 125428 (2006).
17. P. G. Collins, M. S. Arnold, Ph. Avouris, *Science* **292**, 706 (2001).
18. P. G. Collins, M. Hersam, M. Arnold, R. Martel, Ph. Avouris, *Phys. Rev. Lett.* **86**, 3128 (2001).
19. B. Bourlon *et al.*, *Phys. Rev. Lett.* **92**, 026804 (2004).
20. Most of the low-resistive devices engineered with the electrical-breakdown technique can be actuated with an electron current, although this is never the case for the non-engineered devices (*21*).
21. Materials and methods are available as supporting material on *Science* Online.
22. M. F. Yu, B. I. Yakobson, R. S. Ruoff, *J. Phys. Chem. B* **104**, 8764 (2000).
23. A. Kis, K. Jensen, S. Aloni, W. Mickelson, A. Zettl, *Phys. Rev. Lett.* **97**, 025501 (2006).
24. E. R. Kay, D. A. Leigh, F. Zerbetto, *Angew. Chem. Int. Ed.* **46**, 72 (2007).
25. S. Chen *et al.*, *Appl. Phys. Lett.* **87**, 263107 (2005).
26. G. S. Kottas, L. I. Clarke, D. Horinek, J. Michl, *Chem. Rev.* **105**, 1281 (2005).
27. G. E. Begtrup *et al.*, *Phys. Rev. Lett.* **99**, 155901 (2007).
28. We do not observe any change of the electron resistance when comparing samples with and without gold cargoes. As a result, we do not expect a substantial modification of the spatial temperature profile in these two configurations. A direct consequence of this temperature profile is that the speed of the cargo is not constant along the nanotube. It is highest near the midpoint of the tube and lowest near the contacts (fig. S2).
29. The temperature profile is likely to be slightly asymmetric with respect to the middle of the nanotube resulting from, for example, different contact resistances. As a result, the mobile element can move even if it is placed exactly in the middle of the nanotube.
30. J. Tersoff, *Phys. Rev. Lett.* **61**, 2879 (1988).
31. M. G. L. van den Heuvel, C. Dekker, *Science* **317**, 333 (2007).

32. We thank J. Llobet, G. Rius, and X. Borrisé for valuable help with the experiments, as well as P. Ordejon and M. Monthioux for discussions. Financial support from a European Young Investigator grant, the European Union–funded project FP6-IST-021285-2, the grants FIS2006-12117-C04 and TEC2006-13731-C02-01 from the Ministerio de Educación y Ciencia, a Ramón y Cajal Fellowship, and the grant 2005SGR683 from Agència de Gestió d'Ajuts Universitaris i de Recerca is acknowledged. The work in Lausanne was supported by the Swiss NSF and its National Centres of Competence in Research "Nanoscale Science."

Supporting Online Material

www.sciencemag.org/cgi/content/full/1155559/DC1
Materials and Methods
Figs. S1 to S5
Tables S1 and S2
References
Movies S1 to S5

22 January 2008; accepted 31 March 2008
Published online 10 April 2008;
10.1126/science.1155559
Include this information when citing this paper.

Fracture Propagation to the Base of the Greenland Ice Sheet During Supraglacial Lake Drainage

Sarah B. Das,[1*] Ian Joughin,[2] Mark D. Behn,[1] Ian M. Howat,[2,3] Matt A. King,[4] Dan Lizarralde,[1] Maya P. Bhatia[5]

Surface meltwater that reaches the base of an ice sheet creates a mechanism for the rapid response of ice flow to climate change. The process whereby such a pathway is created through thick, cold ice has not, however, been previously observed. We describe the rapid (<2 hours) drainage of a large supraglacial lake down 980 meters through to the bed of the Greenland Ice Sheet initiated by water-driven fracture propagation evolving into moulin flow. Drainage coincided with increased seismicity, transient acceleration, ice-sheet uplift, and horizontal displacement. Subsidence and deceleration occurred over the subsequent 24 hours. The short-lived dynamic response suggests that an efficient drainage system dispersed the meltwater subglacially. The integrated effect of multiple lake drainages could explain the observed net regional summer ice speedup.

The Greenland Ice Sheet flows outward from its interior through a combination of internal deformation and basal sliding, losing mass around its edges through meltwater runoff and iceberg calving. Recent observations show that ice flow along the western margin accelerates during the summer when surface meltwater lubricates sliding at the ice-bedrock interface (*1*, *2*). Aside from theoretical predictions (*3*–*5*) and observations on small icecaps (*6*), it has not been established how surface meltwater penetrates through thick, subfreezing ice (*7*, *8*). Ice-sheet models used to predict future sea-level rise typically do not include the impact of surface meltwater on ice dynamics. Attempts to include the effects of enhanced basal lubrication within these models suggest that increased meltwater may substantially accelerate ice-sheet mass loss, but confidence in these results is limited by a poor understanding of ice-sheet hydrology (*9*). Key unknowns in determining Greenland's potential response to climate forcing are the time scales and pathways through which meltwater reaches the ice sheet's base and its consequent effect on basal motion (*10*).